Volume 1 | Number 1 | Jan 2013 | Pages 1–100

Nanoscale

www.rsc.org/nanoscale

ROYAL SOCIETY OF CHEMISTRY

ROYAL SOCIETY OF CHEMISTRY

www.rsc.org/nanoscale

Novel Peapoded Li$_4$Ti$_5$O$_{12}$ Nanoparticles for High-rate and Ultralong-life Rechargeable Lithium Ion Batteries at Room and Lower Temperatures

Liang Peng, Huijuan Zhang, Ling Fang, Yan Zhang, Yu Wang*

The State Key Laboratory of Mechanical Transmissions and School of Chemistry and Chemical Engineering, Chongqing University, Chongqing 400044, China

E-mail: wangy@cqu.edu.cn; prospectwy@gmail.com

Keywords: mesoporous, lithium titanate (Li$_4$Ti$_5$O$_{12}$), carbon shell, rate capability, lithium ion batteries.

Abstract

In this paper, a novel peapod-like Li$_4$Ti$_5$O$_{12}$-C composite architecture with high conductivity is firstly designed and synthesized to be used as anode materials for lithium-ion batteries. In the synthesis, Na$_2$Ti$_3$O$_7$ nanotubes act as precursors and sacrifical templates, and glucose molecules serve as the green carbon source, thus the peapod-like Li$_4$Ti$_5$O$_{12}$-C composite can be fabricated by a facile hydrothermal reaction and the subsequent solid-state process. Compared to the previous reports, the as-prepared samples obtained by our new strategy exhibit excellent electrochemical performances, such as outstanding rate capability (an extremely reversible capability of 148 mAh g^{-1}, 125 mAh g^{-1} at 30 C and 90 C, respectively) and as well as excellent cycling performance (about 5% capacity loss after 5000 cycles at 10 C with 152 mAh g^{-1} capacity retained). The low-temperature measurements also demonstrate that the electrochemical performances of the peapod-like Li$_4$Ti$_5$O$_{12}$-C composite are remarkably improved at varies rate current (at the low-temperature of -25℃, a high Coulombic efficiency of about 99% can be achieved after 500 cycles at 10 C).

Introduction

Lithium-ion batteries (LIBs), especially with high rate, long life and high energy density properties, are of major superiority for most practical applications, such as portable electric devices and electric vehicles.[1-3] However, to further enhance the power and energy density, lifetime, and safety, new electrode materials and novel structures with a higher specific capacity and more stable charge-discharge cycling capability are required for LIBs.[4, 5] Graphitic carbon is commonly used as anode material in most commercial LIBs, but the rate performance and cycling capability are poor due to forming the solid electrolyte interphase film (SEI) during Lithium-ion (Li-ion) insertion/extraction process.[6, 7] As a potential electrode material, the spinel-type $Li_4Ti_5O_{12}$ has been demonstrated as the most promising anode material for LIBs. The spinel $Li_4Ti_5O_{12}$ possesses a comprehensively high operating voltage ~1.55 V ($vs.$ Li/LI$^+$) which could avoid the formation of the SEI and lithium dendrites to partly ensure the safety of the LIBs.[8, 9] Furthermore, its unique spinel frame structure can provide stable 3-D network channels which contribute to Li$^+$ diffusion, resulting in excellent Li$^+$ insection/extraction reversibility and structural stability.[8]

Despite these advantages described above, it still remains some challenges caused by poor electronic conductivity ($S_{Li4Ti5O12} < 10^{-13}$ S cm^{-1}) and sluggish Li-ion diffusion coefficient (10^{-9}-10^{-13} cm^{-2} s^{-1}).[3, 10] In order to overcome the above drawbacks, various efforts have been developed to fabricate composites with different structures to improve the battery performance, such as nanostructured particles,[8, 11] hollow microsphere,[12] mesoporous microsphere,[13] flower-like nanosheet,[14] etc. These prepared nanostructured $Li_4Ti_5O_{12}$ based anode materials demonstrated significant enhancement in rate performance. However, the electronic conductivity of the nanostructured materials is still low.

Because its impressive chemical and physical properties, the graphitized carbon is wildly used to enhance the materials conductivity and the same time avoiding the electrolyte direct contact with the electrode, enabling enhanced rate performance and cycling capacity of LIBs.[15, 16] After carbon coating, the composites can display a synergic effect that is derived from the unique nanostructure composite and are

therefore able to present better performances than the corresponding materials in pure phase. Recently, several efforts have already been tried to apply the carbon coating, for example, Li *et al.* introduced the $Li_4Ti_5O_{12}$/carbon composite with a lump morphology by hydrothermal process and following heat treatment.[8] shen et al. prepared a $Li_4Ti_5O_{12}$/carbon nanocomposite with a core–shell structure by a solid-state reaction.[17, 18] Zhu et al reported a nanoporous $Li_4Ti_5O_{12}$/carbon micro-sphere.[13] All of these harvested materials exhibit good rate performance and excellent cycling capability. However, these materials still show apparent drawbacks such as high irreversible capacity loss and low energy and power density, due to the larger sample size and the aggregation of the active materials. For most of $Li_4Ti_5O_{12}$ based anode materials, it is still a great challenge that as-prepared materials own both the wonderful nanostructures and super electron conductivity for power batteries with high energy density and excellent rate performance. Meanwhile, keeping in mind that some practical applications LIBs are likely to use at very low temperature, so we believe that the improvement of the low temperature performance of electrodes for LIBs represent nowadays a big challenge too.

In this paper, we introduce a facile method to uniquely synthesize an encapsulated carbon based composite, which is made up of $Li_4Ti_5O_{12}$ nanoparticles dispersed inside and carbon fiber/tubes encapsulating outside. With this special nanostructure, the functional nanoparticles tightly surrounded and protected by the carbon shell and therefore can prevent the $Li_4Ti_5O_{12}$ nanoparticles from aggregating and pulverizing, and thereby keep the primary nanofiber/tube morphology during charge-discharge process, which results in excellent rate and cycling performances. Both of the obtained peapod-like nano-sized $Li_4Ti_5O_{12}$–Carbon composite (NS-LTO-C) and macro-sized $Li_4Ti_5O_{12}$ composite (MS-LTO) are measured electrochemical performances at room and low-temperature (25℃, 0℃, -25℃), respectively.[19, 20] When tested at room temperature, the as-prepared NS-LTO-C composite exhibits a high capacity (a reversible capability of 162 mAh g^{-1}, 157 mAh g^{-1}, 148 mAh g^{-1} at 5 C, 10 C and 30 C, respectively) and a super cycling performance (only 3 % capacity loss after 5000 cycles at 10 C current density with a capacity retention of 152 mAh

g^{-1}). The low-temperature measurements also demonstrate that the electrochemical performances of the NS-LTO-C composite are remarkably improved at varies rate current (at the temperature of -25℃, a high Coulombic efficiency of about 99% can be obtained after 500 cycles at 10 C).

Experimental Section

Materials: All materials or chemicals were used as received and analytical grade. anatase TiO_2 (99.9%, Aldrich), NaOH (99.9%, Aldrich), HCl (37 Wt%, J.T.Baker), Li_2CO_3 (98%, AR), D(+)-glucose (Cica-Reagent, Kanto Chemical) and metallic Li foil (99.9%, Aldrich).

Synthesis of Titanic Acid ($H_2Ti_3O_7$) nanotubes

To synthesize the precursor $H_2Ti_3O_7$ (HTO) nanotubes, we select the commercial anatase TiO_2 as the original reactant. In a typical synthesis, 1.0 g of the anatase TiO_2 with 40 mL of 10 M NaOH put into a 50 mL Teflon-lined autoclave at 150℃ in an electric oven for 24 h.[21, 22] After the thermal treatment and subsequent cooling to room temperature naturally, the precipitates were filtered and washed with distilled water until pH~7, and then added 0.1 M HCl aqueous solution to adjust acid-base property until the PH~1. After that, the suspension was gently stirred for 8 h, and then the as-prepared samples washed with distilled water and absolute ethanol until no Cl^- can be detected. The precursor nanotube samples were attained after dried in an oven at 60℃ for 12 h.

Synthesis of the peapod-like NS-LTO-C composite.

To synthesize the NS-LTO-C composite, three steps were involved: firstly, 100 mg $H_2Ti_3O_7$ nanotubes were uniformly mixed with 35 mL glucose aqueous solution (0.15 M), then transferred into a 50 mL Teflon-lined autoclave and subsequently put into an electric oven at 180 ^{o}C for 8 hours. After that, the samples were washed at least three times using deionized water and pure ethanol, and then dried in a vacuum drying oven at 60 ^{o}C overnight to remove the residue water and ethanol. Secondly, the carbonized glucose coated $H_2Ti_3O_7$ nanotubes were annealed at 800 ^{o}C in the Chemical Vapor Deposition (CVD) for 200 min (Ar atmosphere) to obtain the peapod-like TiO_2-C

nanocomposite. Thirdly, the obtained peapod-like TiO_2-C nanocomposite uniformly mixed with Li_2CO_3 (the Li/Ti mole ratio was 0.8) and subsquently calcined at 800 $^{\circ}$C in CVD (Ar atmosphere) for 10 hours to get the peapod-like NS-LTO-C composite.[10, 17]

The MS-LTO composite is synthesized by a conventional solid-state process. The $H_2Ti_3O_7$ nanotubes were directly mixed with Li_2CO_3 (the Li/Ti mole ratio was 0.8) and then annealed at 800 $^{\circ}$C in the CVD for 10 hours (Ar atmosphere) to obtain the MS-LTO composite.

Material Characterizations.

The fabricated materials were characterized by powder X-ray diffraction (Bruker D8 Advance X-ray diffractometer) with Cu Kα radiation, scanning electron microscope (SEM, JEOL, JSM-7800F) with an energy dispersive spectrometer (EDS), transmission electron microscopy (TEM, JEOL, JEM-2100F), Brunauer-Emmett-Teller surface-area and pore-size analyzer (BET, Quantachrome Autosorb-6B)andRaman spectroscopy (RENISHAW Invia Raman Microscope, voltage (AC) 100-240 V, power 150 W).

Electrochemical Measurements

Electrochemical measurements were performed with R2032 coin-type cells. A homogeneous mixture composed of either the active material with a carbon black conducting agent and a polyvinyl difluoride (PVDF) using 1-methyl-2-pyrrolidinone (NMP) as a solvent in a weight ratio of 80:10:10 were prepared under strong magnetic stirring for 3 days. Then the mixture was extracted and spread on Cu foils as working electrodes (Figure S4). After drying, the mass loading of the mixture on Cu foil is about 12 mg/cm^2. A lithium metal was used as the counter and reference electrode and a Celgard 2400 membrane was used as the cell separator. The electrolyte was 1 M $LiPF_6$ in ethylene carbonate and diethyl carbonate (EC-DEC, v/v=1:1). The cells were constructed in an Ar-filled glove box. The galvanostatic cycling was performed on Neware battery testing system, and cyclic voltammetry (CV) was collected using Autolab (model of AUT71740). The electrochemical impedance measurements were carried out by applying an AC voltage of 5 mV in the frequency from 0.01 Hz to 100

kHz. The specific capacity and current density were calculated based on the mass of the active material in the working electrode. The electrochemical tests were carried out using a three electrode system at the temperature range from 25 $^{\circ}$C to -25°C. A digital low temperature biochemical incubator was used to provide different temperatures for the low temperature electrochemical measurements.

Results and Discussion

Synthetic processes

Scheme 1 illustrates synthesis processes and obtained architectures of our samples by the procedure developed in this new strategy and conventional solid-state approach. Different from the conventional process where only micro-sized mesoporous $Li_4Ti_5O_{12}$ composite (MS-LTO) can be obtained, our new strategy for preparing the peapod-like nano-sized mesoporous $Li_4Ti_5O_{12}$-carbon composite (NS-LTO-C) can be briefly described in Scheme 1a and the details can be found in the Experimental Section. The synthesis of our peapod-like sample involves three steps: firstly, the $H_2Ti_3O_7$ (HTO) nanotubes are prepared by a hydrothermal reaction and subsequent H^+ exchange process($3TiO_2 + 2NaOH \rightarrow Na_2Ti_3O_7 + H_2O$; $Na_2Ti_3O_7 + H^+ \rightarrow H_2Ti_3O_7 + Na^+$),[9] and then coated by a carbonized glucose layer by a secondary hydrothermal process with glucose molecules as an organic carbon source. Secondly, the glucose-coated HTO nanotubes are calcined in an Ar atmosphere at a setting temperature to generate the intermediate product, the peapod-like mesoporous TiO_2-carbon composite ($H_2Ti_3O_7 \rightarrow 3TiO_2 + H_2O$; $C_6H_{12}O_6 \rightarrow 6C + 6H_2O$). Thirdly, the above mentioned intermediate samples are homogeneous mixed with the proper ratio of the lithium source (Li_2CO_3) and follow annealed in inert atmosphere ($Li_2CO_3 \rightarrow Li_2O + CO_2$; $2Li_2O + 5TiO_2 \rightarrow Li_4Ti_5O_{12}$).[23] Because the peapod-like TiO_2-C composite own the a great many mesopores, the molten Li_2O can easily diffuses through the mesoporous carbon layers to react with the TiO_2 particles during the calcination process, and the uniform and continuous carbon shells can effectively limit the reaction area thereby avoiding TiO_2 or $Li_4Ti_5O_{12}$ particles growth and

6

aggregation, resulting in obtaining the peapod-like NS-LTO-C composite.

Structure and morphology Characterizations

The precursors for fabricating the peapod-like NS-LTO-C composite are $H_2Ti_3O_7$ (HTO). Scanning electron microscopy (SEM) and transmission electron microscopy (TEM) are applied to present the morphological and structure of so-collected precursors (Figure 1). The typical SEM image (Figure 1a) reveals that the samples could be fabricated in large scale and shown uniformly 1-D nanostructure in our experiments. To obtain more details about the precursors, TEM is used to disclose more information of morphology (Figure 1b,c,d). From the representative TEM image, it can be clearly seen that the samples exhibit uniform tube-shaped morphology (Figure 1b).[24] The locally magnified TEM image (Figure 1c), detects that these tube-shaped samples are 10-20 nm in width and extremely thin in tube wall, which is in favor for the formation of the peapod-like morphology during finally two-steps anneals. Actually, the peapod-like feature inherits and develops from the morphology of TiO_2-C composite (Figure S1). High-resolution TEM (HRTEM) analysis (Figure 1d) represents that the crystal inter-lattice which corresponds to (200) crystal plane for $H_2Ti_3O_7$ is 0.786 nm.[25, 26] Both the uniform morphology and single crystal nature can provide strong guarantees for the successfully synthesis peapod-like NS-LTO-C composite.

The X-ray diffraction (XRD) characterizations are collected to trace the overall conversion process (Figure 2). From bottom to top, three distinct XRD patterns correspond to $H_2Ti_3O_7$ (JCDPS 36-654), TiO_2 (JCPDS 21-1276)[27], $Li_4Ti_5O_{12}$ (JCPDS 49-0207)[3], respectively, indicating the total conversion process involved from the precursors to the intermediate samples, and to the desired products in the end. However, no peaks of carbon can be indexed in the peapod-like NS-LTO-C composite XRD pattern, which is mostly due to the amorphous structure or the low content of carbon. While the EDS pattern (Figure S2) reveals that the samples mainly contain C, O and Ti elements as well as demonstrate the carbon presence in the finally composite.

The SEM and TEM are also carried out to investigate the as-prepared peapod-like samples (Figure 3). The low-magnification SEM image (Figure 3a) reveals that, under typical condition, abundant peapods can be prepared. The enlarged SEM image (Figure 3b) shows that the regular one-dimensional (1-D) peapod structures are aligned together and the encapsulated $Li_4Ti_5O_{12}$ nanoparticles clearly appear and distribute along the 1-D structures. In contrast, the SEM image (Figure S3) about the MS-LTO composite demonstrates non-uniform and aggregated particles exited in the sample. The typical TEM images (Figure 3c,d) are used to collect more information about the unique structures for our samples. From both images, especially in image d, it is detected that the $Li_4Ti_5O_{12}$ nanoparticles with ~ 10-20 nm in diameter are uniformly dispersed along the same direction of carbon fibers with periodic intervals. The magnified TEM image (Figure 3e) distinctively shows two $Li_4Ti_5O_{12}$ nanoparticles encapsulated in the carbon fiber, which contains some observations of mesopores on the surface with diameters of about 2-4 nm. The locally enlarged HRTEM image (Figure 3f) reveals one interplane with lattice space of 0.481 nm, match very well with the (111) crystal planes for spinal $Li_4Ti_5O_{12}$.[28, 29] The corresponding FFT pattern is shown in the inset of panel f, displaying the nature of single-crystallinity in these $Li_4Ti_5O_{12}$ nanoparticles.[30, 31] X-ray photoelectron spectroscopy (XPS) analysis of the NS-LTO-C composite is conducted from 0 to 1200 eV (Figure S5). Obvious O1s, Ti2p and C1s peaks are detected, and corresponding high resolution spectra are shown.

The Raman spectra of the samples are applied to investigate the state of carbon. As we know, the D band peak expresses the disordered graphitic crystal stacking as well as the G band indicates the corresponding ordered graphitic crystal stacking.[32, 33] The Raman spectra (Figure 4a) of the NS-LTO-C composite are consisted of two main bands at around 1357 and 1597 cm^{-1}, which are considered to be the D band and G band, respectively. The degree of crystallization of the carbon fiber can be determined by evaluating the value I_D/I_G (the peak intensity ratio). A lower value of I_D/I_G parameter corresponds to a higher degree of crystallization. The value of the I_D/I_G ratio for NS-LTO-C is less than 1, which suggests that the crystallization of the carbon

is relatively high.[34] Unlike the MS-LTO composite, the peapod-like NS-LTO-C composite has low I_D/I_G ratio value, indicating better crystallization by two steps annealing at the high temperature. Nitrogen absorption/desorption analysis also are applied to reveal the Brunauer-Emmett-Teller (BET) surface areas (Figure 4b) and pores-size distributions (Figure 4c) of the NS-LTO-C and MS-LTO composite. The specific surface area for the peapod-like NS-LTO-C composite could reach up to 154.4 m^2 g^{-1}, which is useful for electrolyte to completely permeate into the samples and consequently proceed with fast Lithium ion charge/discharge, however, the specific surface area for MS-LTO is only 17.2 m^2 g^{-1}, the pore-size mainly distribute at 4.6 and 5.9 nm, which also are favorable for the soak and diffusion of the electrolyte. In fact, the coated carbon layers with porous structure are very important for the formation of the peapods, while the property of mesoporousity could be reasonably inferred from the relief of CO, CO_2 and H_2O by the $H_2Ti_5O_7$ and the thermal decomposition of the carbonization layers.

Electrochemical characterizations

The theoretical capacity of spinel $Li_4Ti_5O_{12}$ depends on its 3D crystal structure. $Li_4Ti_5O_{12}$ can accommodate 3 Li-ion and consequently get a chemical formula of $Li_7Ti_5O_{12}$ with a theoretical capacity of 175 mAh g^{-1}($Li_4Ti_5O_{12}$ + $3Li^+$ + $3e^{-1}$ ↔ $Li_7Ti_5O_{12}$).[35] As shown in Figure 5, the spinel-type $Li_4Ti_5O_{12}$, belongs to the *Fd3m* space group, whose Li-ions occupy octahedral (16d) and tetrahedral (8a) sites ($[Li]_{8a}[Li_{1/3}Ti_{5/3}]_{16d}[O_4]_{32e}$).[4, 36] . The intercalation process occurred along varied Li diffusion paths such as 8a-16c-8a and 8a-16c-48f-16d inside the above mentioned original formula unit, enabling obtain the rock salt structure type of $Li_7Ti_5O_{12}$ ($[Li_2]_{16c}[Li_{1/3}Ti_{5/3}]_{16d}[O_4]_{32e}$). In this intercalation process, a negligible volume change of only 2% is caused between both end members of $Li_4Ti_5O_{12}$ and $Li_7Ti_5O_{12}$ accompanied by a change of the lattice axis from 8.3595Å to 8.3538Å, and as a result it is a "zero-strain" electrode material with superior rate performances and excellent cycling capacity.[37, 38]

The electrochemical performances of the peapod-like NS-LTO-C composite and the MS-LTO composite are systematically measured using the typically coin cells. The

cyclic voltammetry (CV) curve (Figure 6a) for the peapod-like NS-LTO-C composite is reversibly scanning from 1.0 to 3.0 V (*vs.* Li/Li$^+$) in five cycles. The excellent stability in current densities and potential positions between the second and five cycles clearly indicate that the fast and reversible Li$^+$ insertion/extraction during charge/discharge process. The rate performances of the peapod-like NS-LTO-C composite exhibited in Figure 6b were tested at the current rates of 0.2-90 C over a potential window of 1.0-3.0 V (*vs.* Li/Li$^+$). At the initial lower rate of 0.2 C (35 mAh g^{-1}), the NS-LTO-C composite displays an extremely flat voltage plateau at the potential of ~ 1.55 V and the discharge capacity can reach to 172 mAh g^{-1}, and when the current density gradually increased to 1, 5, 10 and 30 C, correspondingly, the discharge capacity can be stably delivered 172, 162, 157 and 148 mAh g^{-1}, respectively. Even the rate current density increases up to 90 C, the electrode still delivers a discharge capacity of 125 mAh g^{-1} and this value is approximately 71.4% of the theory capacity (175 mAh g^{-1}). Compared with the previous reports, the peapod-like sample reveals best electrochemical performances at various rate current (the details shown in the Table 1).To investigate the cycling performance of the NS-LTO-C composite, our samples were carried out galvanostatic measurement with the high rate of 10 C upon 500 cycles. The results (Figure 6c) show that the initial discharge capacity of the NS-LTO-C composite is 157 mAh g^{-1}, and the retained discharge capacity after 5000 cycles are 152 mAh g^{-1}. The capacity retention ratio of the NS-LTO-C composite at a high rate of 10 C can reach up to 96.8%, which is better than that of the most previous reports,[8, 23, 39] and the corresponding Coulombic efficiency remains constant at ~100%.

To investigate the discharge capacities against different current densities for the peapod-like NS-LTO-C composite, each of them sustain for 20 cycles at different current densities (Figure 6d). The results reveal that the cyclic performances are stable for all rates and a discharge capacity of ~ 164 mAh g^{-1} can be obtained when the current density reduced back to 1 C after 100 cycles at high rates. Compared to the MS-LTO composite, the peapod-like NS-LTO-C composite exhibits a much better rate capability and much higher storage capacity (Figure 6e), for example, when the rate

increase to 90 C, the capacity of the NS-LTO-C composite is approximately 3 times greater than that of the MS-LTO-C composite. Electrochemical impedance spectroscopy (EIS) is conducted to investigate the conductivity of interfacial processes and charge transport between the material and electrolyte. The Nyquist plots (Figure 6f) for the peapod-like NS-LTO-C composite and the MS-LTO composite display a straight line in the low-frequency region and a semicircle in the high-frequency region, which corresponds to the diffusional limited electron-transfer process and electron-transfer-limited process, respectively.[17, 40] From the plots, we can draw a conclusion that the peapod-like NS-LTO-C composite exhibits a lower charge-transfer resistance than the MS-LTO composite, indicating a better conductivity for the peapod-like NS-LTO-C composite.[3, 41]

The low-temperature electrochemical behaviors of the peapod-like NS-LTO-C composite and the MS-LTO composite as anode materials are investigated by galvanostatic charge/discharge, rate performances and cycling performance measurements (Figure 7). The discharge performances of the peapod-like NS-LTO-C composite electrodes at different temperatures ranging from 25 ^{o}C to -25 ^{o}C are tested by galvanostatic charge/discharge between 1.0-3.0V (vs Li/Li$^+$) at the current density of 0.2 C (Figure 7a). With the temperatures decreasing, the discharge capacities of the two anode materials display expectedly diminished. Meanwhile, it can be found that the ratios of the discharge capacity at -25 ^{o}C and 0 ^{o}C to the value at 25 ^{o}C at the rate of 0.2 C correspondingly 95.9% and 98.8% for the NS-LTO-C composite and that are 91.0% and 96.4% for the MS-LTO composite, respectively. The reported low-temperature capacities obtained at a relatively low rate partly indicate that the unique peapod-like nanostructure in the electrode formulation is beneficial for improving the electrochemical performance at the low-temperature. At the low-temperature (-25 ^{o}C), the comparisons of the discharge capacities achieved from the peapod-like NS-LTO-C composite and the MS-LTO composite at different current densities are presented (Figure 7b). From this Figure we can determine that the peapod-like NS-LTO-C composite obviously exhibits a higher storage capacities and improved rate capabilities than the MS-LTO composite, with discharge capacities of

167, 162, 151,133 and 122 mAh g^{-1} at 0.2, 1, 5, 10 and 30C, respectively. However, the MS-LTO composite only maintains discharge capacities of 153, 125, 108, 78 and 24 mAh g^{-1} at corresponding rates currents, respectively. The improved electrochemical properties is mostly likely due to the excellent electronic conductivity for the uniform carbon coating, large specific surface area, nano-size of the active materials and the synergic effect of the unique structure for the peapod-like NS-LTO-C composite.[19, 20, 42] The comparison of the cycling performance of these two composite electrodes at 10 C in the voltage range of 1.0-3.0 V (vs Li/Li$^+$) is shown in Figure 7c. The discharge capacities of the peapod-like NS-LTO-C composite and the MS-LTO composite after 500 cycles are 157 and 61 mAh g^{-1}, indicating 96% and 52% retention of second discharge capacity, respectively. Moreover, after 500 cycles operating at 10 C, the peapod-like NS-LTO-C composite electrode still has a stable electrochemical properties with a high Coulombic efficiency of ~ 99% (Figure 6c), which is extremely higher than that of the MS-LTO composite (~82%).

Actually, this enhanced rate and cycling performances at room and low-temperature could be attributed to these merits: (ⅰ) The novel core-shell nano-structure provides a perfect formation with the active anode material of Li$_4$Ti$_5$O$_{12}$ encapsulated inside graphitized carbon fibers, which can prevent the active nanoparticles from agglomeration and pulverization.[43, 44] (ⅱ) The as-prepared peapod-like nanocomposite with graphitized carbon fiber supporting has a great mechanical toughness, which can effectively alleviate the external pressures during assembling the lithium-ion batteries, resulting in higher energy and volume density. (ⅲ) The high specific surface area (154.43 m^2 g^{-1}), particularly a large quantity of reaction sites exposing outside, would effectively enlarge the contact areas and lithium exchange during electrochemical tests.[45] (ⅳ) The Li$_4$Ti$_5$O$_{12}$ nanoparticles with the small diameters of 20-30 nm would greatly accelerate the charge/discharge of lithium and shorten the charge transfer pathway and lower the resistance for Li-ion between active materials and electrolyte.[46, 47] (ⅴ) The synergic effect between the active-material core and carbon–fiber shell would also improve the rate and cycling performances during charge/discharge process for lithium-ion batteries. All of the

advantages mentioned above imply and support one predictable result that our samples with the unique structure will demonstrate excellent electrochemical performance for lithium-ion batteries.

Conclusion

In summary, in this article, we report a new and rational strategy towards synthesize one kind of novel $Li_4Ti_5O_{12}$-carbon composite peapod-like structure, and applied in the electrochemical test of lithium-ion batteries. Owing to the unique mesoporous peapod-like structure, the material presents several advantages, such as excellent conductivity, high contact surface area, shortened Li-ion diffusion distance and great structure stability. Therefore, the peapod-like NS-LTO-C composite exhibits an outstanding rate capability (an extremely reversible capability of 148 mAh g^{-1}, 125 mAh g^{-1} at 30C and 90C, respectively) as well as excellent cycling performance (about 3% capacity loss after 5000 cycles at 10 C with 152 mAh g^{-1} capacity retained). The low-temperature measurements also declare that the electrochemical performances of the peapod-like NS-LTO-C composite are remarkably improved when compared with the MS-LTO composite at varies rate current (a high Coulombic efficiency of about 99% can be obtained after 500 cycles at 10 C). All of these suggests that our peapod-like samples is beneficial to improving the overall electrode activity and kinetics process, and the peapod-like samples also are expected to open up new opportunities for $Li_4Ti_5O_{12}$ to power flexible electronic devices, even at low temperature.

tory for Molecular Sciences (BNLMS) and Hundred Talents Program at Chongqing U

niversity (Grant No. 0903005203205).

Supporting Information Available: More SEM, EDS, TEM, XPS date are available

in the supporting information for this paper.

References

1. N. Oyama, T. Tatsuma, T. Sato and T. Sotomura, *Nature*, 1995, **373**, 598-600.

2. P. Poizot, S. Laruelle, S. Grugeon, L. Dupont and J. M. Tarascon, *Nature*, 2000, **407**, 496-499.

3. M. M. Rahman, J.-Z. Wang, M. F. Hassan, D. Wexler and H. K. Liu, *Adv. Energy Mater.*, 2011, **1**, 212-220.

4. G.-N. Zhu, Y.-G. Wang and Y.-Y. Xia, *Energy Environ. Sci.*, 2012, **5**, 6652-6667.

5. V. Aravindan, J. Gnanaraj, Y. S. Lee and S. Madhavi, *Chem Rev*, 2014, **114**, 11619-11635.

6. T. Cassagneau and J. H. Fendler, *Adv. Mater.*, 1998, **10**, 877-881.

7. M. Yoshio, H. Y. Wang and K. Fukuda, *Angew. Chem. Int. Ed.*, 2003, **42**, 4203-4206.

8. B. Li, C. Han, Y.-B. He, C. Yang, H. Du, Q.-H. Yang and F. Kang, *Energy Environ. Sci.*, 2012, **5**, 9595-9602.

9. L. Cheng, J. Yan, G.-N. Zhu, J.-Y. Luo, C.-X. Wang and Y.-Y. Xia, *J. Mater. Chem.*, 2010, **20**, 595-602.

10. K.-T. Kim, C.-Y. Yu, C. S. Yoon, S.-J. Kim, Y.-K. Sun and S.-T. Myung, *Nano Energy*, 2015, **12**, 725-734.

11. Y. Wang, H. Liu, K. Wang, H. Eiji, Y. Wang and H. Zhou, *J. Mater. Chem.*, 2009, **19**, 6789.

12. Z. Zhang, G. Li, H. Peng and K. Chen, *J. Mater. Chem. A*, 2013, **1**, 15429-15434.

13. G.-N. Zhu, H.-J. Liu, J.-H. Zhuang, C.-X. Wang, Y.-G. Wang and Y.-Y. Xia, *Energy Environm. Sci.*, 2011, **4**, 4016-4022.

14. S. Chen, Y. Xin, Y. Zhou, Y. Ma, H. Zhou and L. Qi, *Energy Environ. Sci.*, 2014, **7**, 1924-1930.

15. H. Q. Li and H. S. Zhou, *Chem. Commun.*, 2012, **48**, 1201-1217.

16. F. L. Lou, H. T. Zhou, T. D. Tran, M. E. M. Buan, F. Vullum-Bruer, M. Ronning, J. C. Walmsley and

D. Chen, *ChemsusChem*, 2014, **7**, 1335-1346.

17.   L. Shen, H. Li, E. Uchaker, X. Zhang and G. Cao, *Nano Lett.*, 2012, **12**, 5673-5678.

18.   T. Yuan, R. Cai and Z. P. Shao, *J. Phys. Chem. C*, 2011, **115**, 4943-4952.

19.   E. Pohjalainen, T. Rauhala, M. Valkeapää, J. Kallioinen and T. Kallio, *J. Phys. Chem. C*, 2015, **119**, 2277-2283.

20.   J. L. Allen, T. R. Jow and J. Wolfenstine, *J. Power Sources*, 2006, **159**, 1340-1345.

21.   A. R. Armstrong, G. Armstrong, J. Canales and P. G. Bruce, *Angew. Chem. Int. Ed.*, 2004, **43**, 2286-2288.

22.   B. L. Tian, X. T. Zhang, S. X. Dai, K. Cheng, Z. S. Jin, Y. B. Huang, Z. L. Du, G. T. Zou and B. S. Zou, *J. Phys. Chem. C*, 2008, **112**, 5361-5364.

23.   H.-G. Jung, S.-T. Myung, C. S. Yoon, S.-B. Son, K. H. Oh, K. Amine, B. Scrosati and Y.-K. Sun, *Energy Environ. Sci.*, 2011, **4**, 1345-1351.

24.   L. Peng, H. Zhang, Y. Bai, Y. Zhang and Y. Wang, *Nanoscale*, 2015, **7**, 8758-8765.

25.   C.-C. Tsai and H. Teng, *Chem. Mater.*, 2006, **18**, 367-373.

26.   B. Zhao, S. Jiang, C. Su, R. Cai, R. Ran, M. O. Tadé and Z. Shao, *J. Mater. Chem. A*, 2013, **1**, 12310-12320.

27.   N. Li, G. Liu, C. Zhen, F. Li, L. L. Zhang and H. M. Cheng, *Adv. Funct. Mater.*, 2011, **21**, 1717-1722.

28.   H. H. Xu, X. L. Hu, Y. M. Sun, W. Luo, C. J. Chen, Y. Liu and Y. H. Huang, *Nano Energy*, 2014, **10**, 163-171.

29.   J. H. Choi, W. H. Ryu, K. Park, J. D. Jo, S. M. Jo, D. S. Lim and I. D. Kim, *Sci. Rep.*, 2014, **4**, 7334.

30.   D. K. Lee, H. W. Shim, J. S. An, C. M. Cho, I. S. Cho, K. S. Hong and D. W. Kim, *Nanoscale Res. Lett.*, 2010, **5**, 1585-1589.

31.   Z. M. Liu, N. Q. Zhang and K. N. Sun, *J. Mater. Chem.*, 2012, **22**, 11688-11693.

32.   W. Li, F. Wang, S. S. Feng, J. X. Wang, Z. K. Sun, B. Li, Y. H. Li, J. P. Yang, A. A. Elzatahry, Y. Y. Xia and D. Y. Zhao, *J. Am. Chem. Soc.*, 2013, **135**, 18300-18303.

33.   C. Wang, Z. Y. Guo, W. Shen, Q. J. Xu, H. M. Liu and Y. G. Wang, *Adv. Funct. Mater.*, 2014, **24**, 5511-5521.

34.   Q. Wei, Q. An, D. Chen, L. Mai, S. Chen, Y. Zhao, K. M. Hercule, L. Xu, A. Minhas-Khan and Q. Zhang, *Nano Lett.*, 2014, **14**, 1042-1048.

35.   L. F. Shen, X. G. Zhang, E. Uchaker, C. Z. Yuan and G. Z. Cao, *Adv. Energy Mater.*, 2012, **2**, 691-698.

36.   W. Schmidt, P. Bottke, M. Sternad, P. Gollob, V. Hennige and M. Wilkening, *Chem. Mater.*, 2015, 1740-1750.

37.   M. Wagemaker, E. R. H. v. Eck, A. P. M. Kentgens and F. M. Mulder, *J. Phys. Chem. B*, 2009, **113**, 224-230.

38.   K. Song, D.-H. Seo, M. R. Jo, Y.-I. Kim, K. Kang and Y.-M. Kang, *The J. Phys. Chem. Lett.*, 2014, **5**, 1368-1373.

39.   Z. S. Hong and M. D. Wei, *J. Mater. Chem. A*, 2013, **1**, 4403-4414.

40.   Y. Wang, H. Rong, B. Li, L. Xing, X. Li and W. Li, *J. Power Sources*, 2014, **246**, 213-218.

41.   L. Peng, Y. Feng, Y. Bai, H.-J. Qiu and Y. Wang, *J. Mater. Chem. A*, 2015, **3**, 8825-8831.

42.   T. Yuan, X. Yu, R. Cai, Y. Zhou and Z. Shao, *J. Power Sources*, 2010, **195**, 4997-5004.

43.   Y. Wang, H. J. Zhang, L. Lu, L. P. Stubbs, C. C. Wong and J. Y. Lin, *ACS Nano*, 2010, **4**, 4753-4761.

44.   Y. Wang, Y. Wang, E. Hosono, K. Wang and H. Zhou, *Angew. Chem. Int. Ed.*, 2008, **47**, 7461-7465.

45.   A. Nugroho, S. J. Kim, W. Chang, K. Y. Chung and J. Kim, *J. Power Sources*, 2013, **244**, 164-169.

46.   W. J. H. Borghols, M. Wagemaker, U. Lafont, E. M. Kelder and F. M. Mulder, *J. Am. Chem. Soc.*, 2009, **131**, 17786–17792.

47.   J. Liu, K. Tang, K. Song, P. A. van Aken, Y. Yu and J. Maier, *Phys. Chem. Chem. Phys.*, 2013, **15**, 20813-20818.

48.   L. Shen, C. Yuan, H. Luo, X. Zhang, K. Xu and Y. Xia, *J. Mater. Chem.*, 2010, **20**, 6998-7004.

49.   J. Haetge, P. Hartmann, K. Brezesinski, J. Janek and T. Brezesinski, *Chem. Mater.*, 2011, **23**, 4384-4393.

50.   L. Shen, C. Yuan, H. Luo, X. Zhang, K. Xu and F. Zhang, *J. Mater. Chem.*, 2011, **21**, 761-767.

51.   J. Liu, K. Song, P. A. van Aken, J. Maier and Y. Yu, *Nano Lett.*, 2014, **14**, 2597-2603.
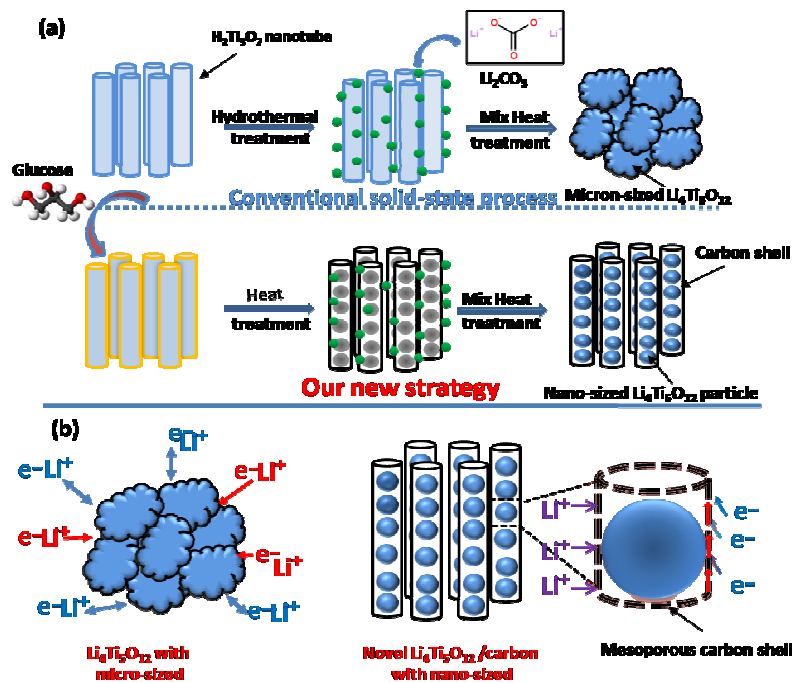
Scheme 1 (a) Schematic presentation of the conventional process for the MS-LTO-C composite and our new strategy for the peapod-like NS-LTO-C composite. (b) Electtron-Transfer pathways of the MS-LTO composite and the peapod-like NS-LTO-C composite.
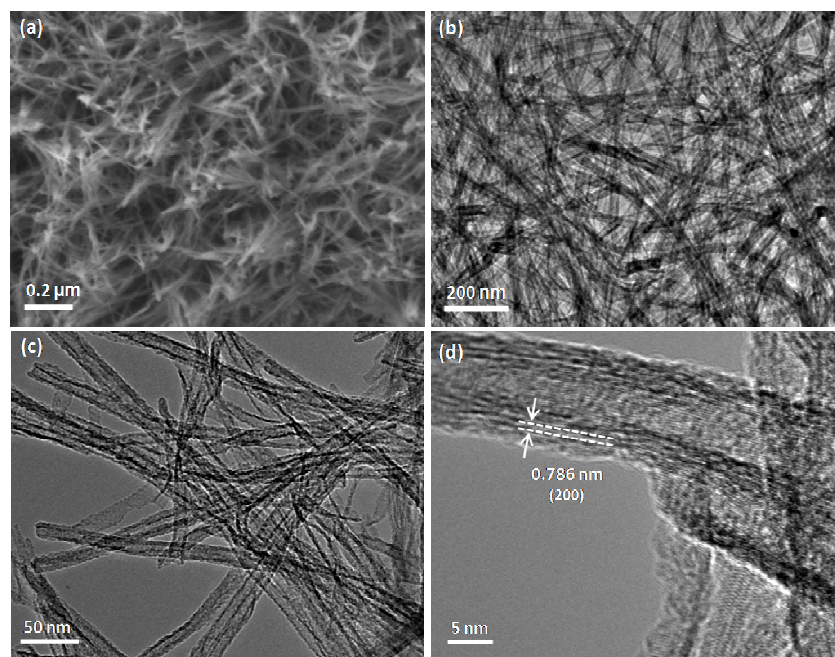
Figure 1 (a) The low-magnification SEM image of the precursor. (b) The low-magnification TEM image to show the tube-shape of the precursor. (c) The locally magnified TEM image to further confirm the nanotube structure and (d) The HRTEM image to characterize the crystal structures of the precursor.
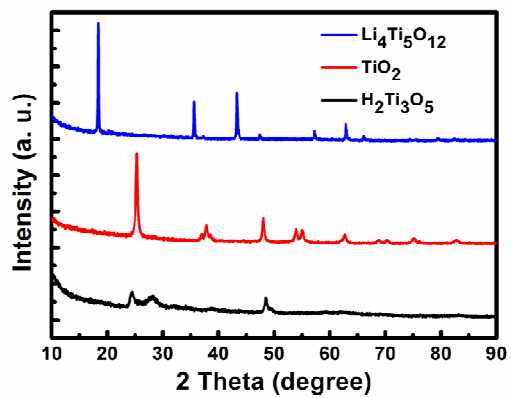
**Figure 2** XRD patterns of the peapod-like NS-LTO-C composite obtained at different synthesis stages.
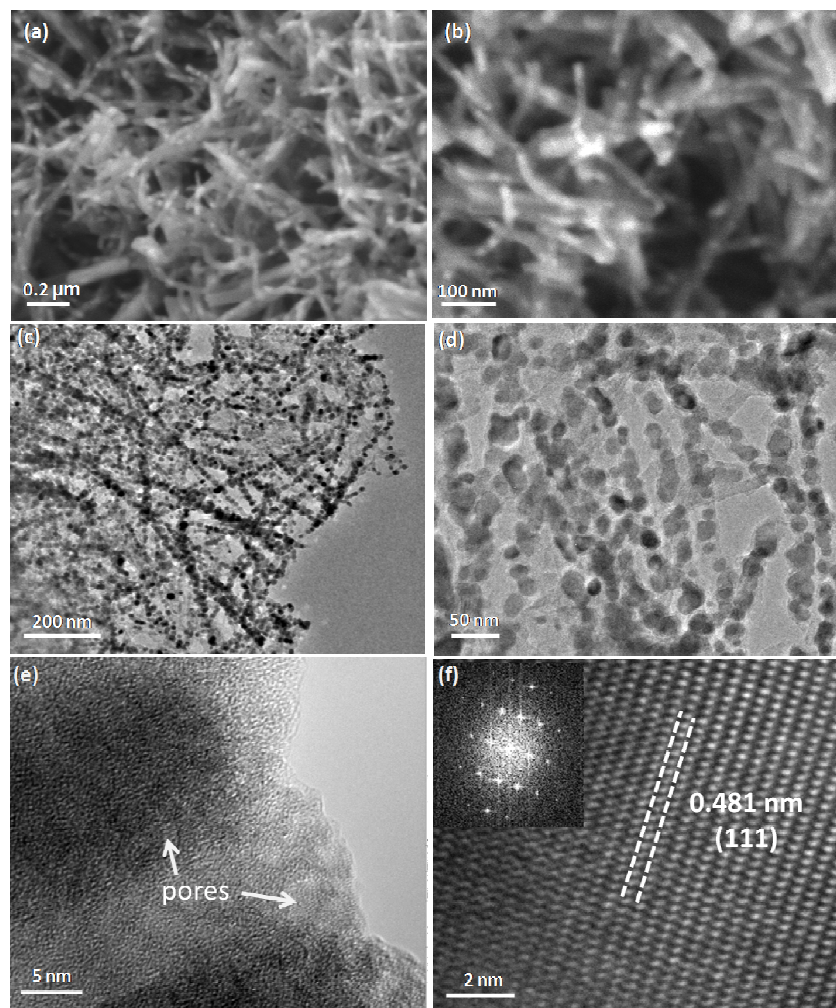
Figure 3 (a) and (b) SEM images of the peapod-like NS-LTO-C nanocomposite. (c) low-magnification TEM image of the final sample. (d) and (e) high-magnification TEM images of the final sample. Inset of (e) is the corresponding FFT pattern. (f) HRTEM image of the as-prepared sample.
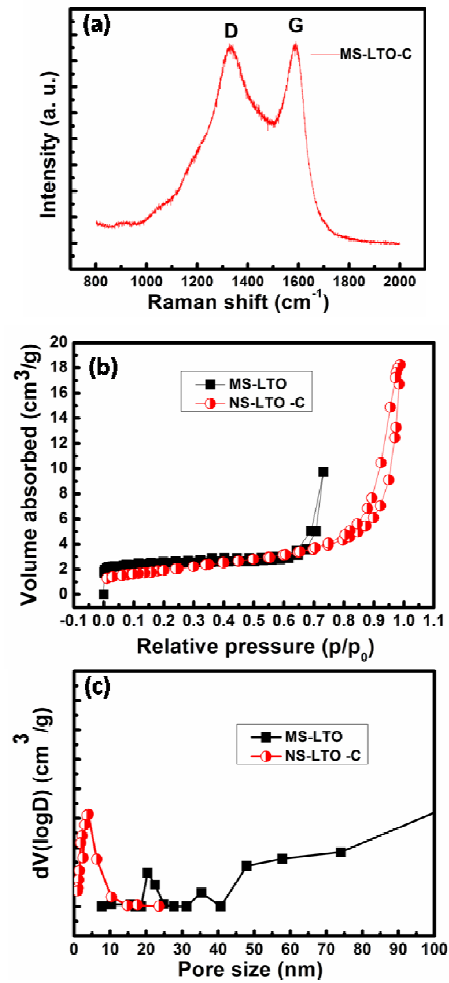
Figure 4 (a) Raman spectra, (b) N_2 adsorption-desorption isotherm and (c) Porous size distributions of the MS-LTO composite and peapod-like NS-LTO-C composite.

Nanoscale Accepted Manuscript
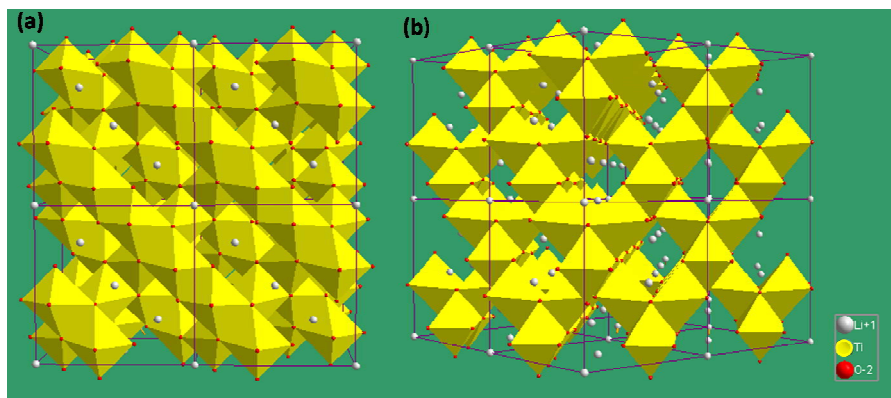
Figure 5 Crystal structure of spinel-type $Li_4Ti_5O_{12}$; the Li ions reside on 16d and 8a sites; oxygen anions occupy 32e positions.
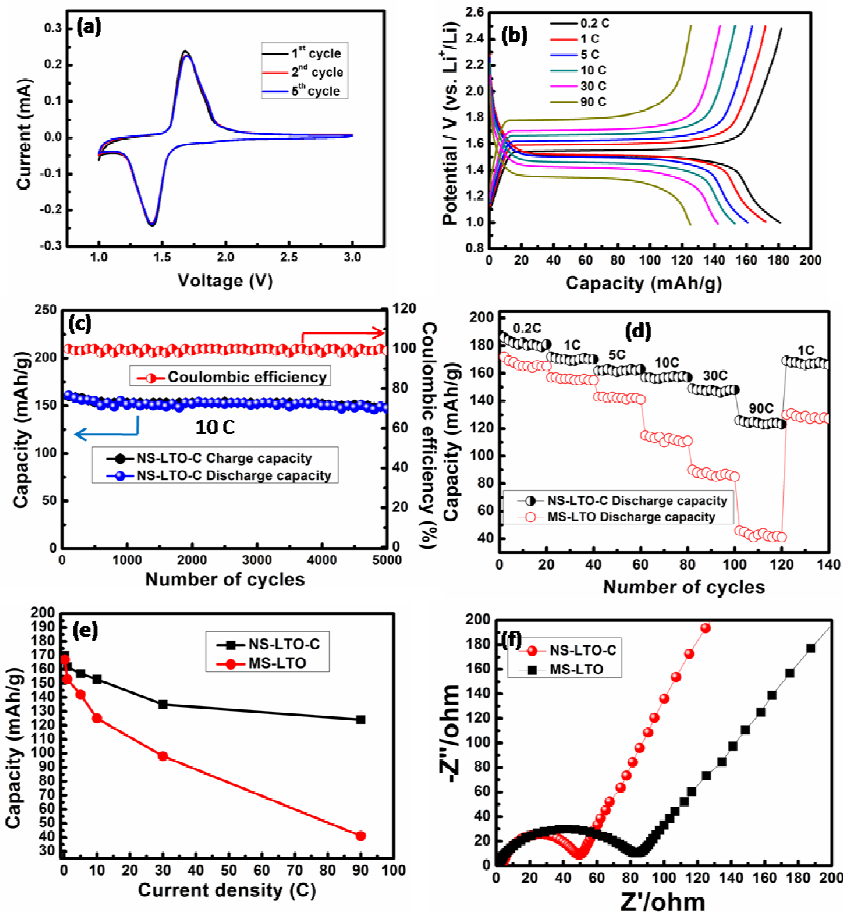
Figure 6 (a) The cyclic voltammetry (CV) profile for the peapod-like NS-LTO-C composite, verifying the thermodynamic stability in electrochemical cycling. (b) The discharge curves at various current densities. (c) The corresponding coulombic efficiency at the current density of 10 C. (d) Rate capability and cycling performances test of the peapod-like NS-LTO-C composite at different current rate. (e) and (f) are the comparisons of the rate capacity retention and Nyquist plots of the MS-LTO composite and peapod-like NS-LTO-C composite.
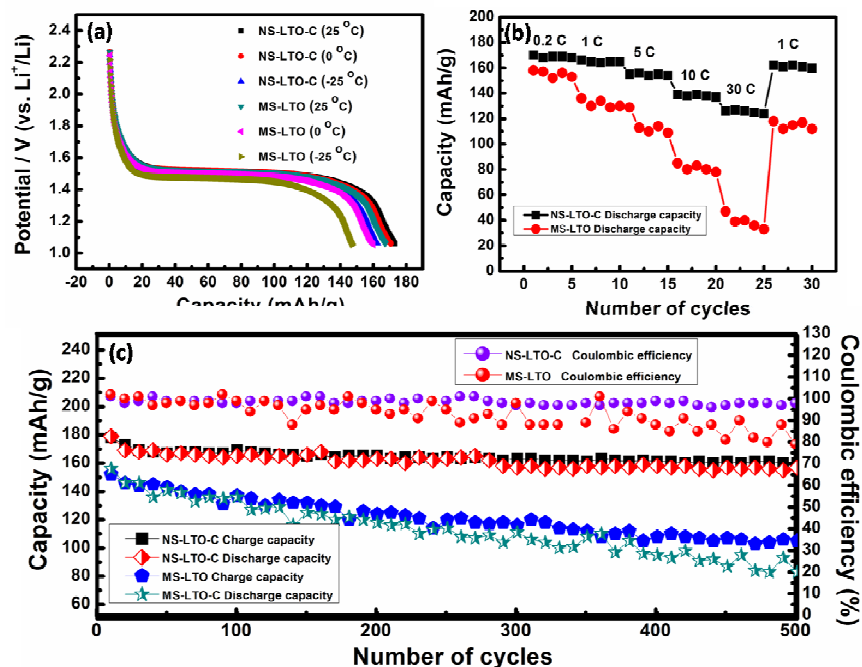
Figure 7 (a) The discharge profiles of the peapod-like NS-LTO-C composite at 1 C rate at different tempeneures. (b) The rate capacity of the peapod-like NS-LTO-C composite at the temperature of -25 $^{\circ}$C. (c) A comparison of the cycling performances and coulombic efficiency of the MS-LTO composite and peapod-like NS-LTO-C composite at 10 C rate at -25 $^{\circ}$C.

Table 1 Comparisons of the electrochemical performance of NS-LTO-C composite with the previous reported results.

Current \ Rate (mA/g) (mAh/g) \ Material	0.2 C	1 C	5 C	10 C	30 C	90 C	References
Porous $Li_4Ti_5O_{12}$ microspheres	167.3	162.4	134.6	116	--	--	48
$Li_4Ti_5O_{12}$/C with a core-shell nanostructure	161	153	146	138	119	85	49
$Li_4Ti_5O_{12}$/C composite	162	152	123	110	~82	--	18
Carbon-coated $Li_4Ti_5O_{12}$ micro-sphere	160	150	138	133	~120	--	13
$Li_4Ti_5O_{12}$ on carbon nanotubes	171.2	158.9	147.8	136.3	--	--	50
$Li_4Ti_5O_{12}$-C nanotube arrays	--	165	--	154	135	~86	51
Peapod-like $Li_4Ti_5O_{12}$-C composite	178	172	162	157	148	125	This work